Modeling the effect of freshwater pulses on the early Holocene climate: The influence of high-frequency climate variability

H. Renssen,[1] H. Goosse, and T. Fichefet

Institut d'Astronomie et de Géophysique Georges Lemaître, Université catholique de Louvain, Louvain-la-Neuve, Belgium

Received 9 April 2001; revised 17 January 2002; accepted 20 January 2002; published 15 May 2002.

[1] The effect of freshwater pulses on the early Holocene climate is investigated with a global coupled atmosphere-sea ice-ocean model. In the model an early Holocene equilibrium climate state is perturbed by releasing a fixed amount of freshwater (4.67×10^{14} m^3) into the Labrador Sea at three different constant rates: 1.5 Sv (1 Sv = 1×10^6 m^3 s^{-1}) in 10 years, 0.75 Sv in 20 years, and 0.3 Sv in 50 years. For each rate, five ensemble experiments have been performed, varying in initial conditions. The freshwater pulses produce a weakening of the thermohaline circulation. The perturbed state is in agreement with proxy evidence for the 8.2 ka event. Two types of recovery of the thermohaline circulation occurred, differing in time-scale: (1) $\leq$200 years and (2) >200 years. In the experiments with 10 year and 20 year pulses, both types of recovery were observed. This suggests that the model response is unpredictable in the range of parameters studied here. It is hypothesized that the unpredictability is associated with annual-to-decadal climate variability. Our results demonstrate that several types of recovery may exist with the same kind of perturbation. The interpretation of events observed in proxy data may be thus more complex than realized until now since the magnitude and duration of climatic events caused by freshwater pulses is likely to depend strongly on nonlinear dynamics inside the coupled atmosphere–sea ice–ocean system. *INDEX TERMS:* 3344 Meteorology and Atmospheric Dynamics: Paleoclimatology; 4255 Oceanography: General: Numerical modeling; 4532 Oceanography: Physical: General circulation; 4215 Oceanography: General: Climate and interannual variability (3309); 9325 Information Related to Geographic Region: Atlantic Ocean; *KEYWORDS:* Holocene, thermohaline circulation, predictability, meltwater, coupled climate model

1. Introduction

[2] Oxygen isotope records derived from Greenland ice cores give convincing evidence for an abrupt cold event (estimated cooling of 3°–6°C over Greenland) that occurred between ~8.4 and ~8.0 calendar kyr B.P., with the maximum deviation at 8.2 calendar kyr B.P. or 7.5 ^{14}C kyr B.P. [*Alley et al.*, 1997]. The event was dubbed the "8.2 kyr event" and represents the most distinct example of rapid climate change during the Holocene. This abrupt anomaly is also registered in other indicators measured in Greenland ice cores, for instance, as a 20% decrease in snow accumulation, a sudden increase in input of dust and sea salt indicating windy conditions, and a marked decrease in methane concentration from ~750 to 600 ppbv [*Blunier et al.*, 1995; *Alley et al.*, 1997; *Chappellaz et al.*, 1997]. Methane variations of this order are thought to have their origin in large-scale climatic shifts, implying that the 8.2 kyr event was not restricted to the North Atlantic region. Probably changes in tropical wetlands played a dominant role [*Raynaud et al.*, 2000]. Indeed, tropical lake level data from Africa and Asia show a sudden and marked lowering around this time, indicative of a strong reduction in precipitation [e.g., *Gasse and Van Campo*, 1994; *Gasse*, 2000]. Evidence for the 8.2 kyr event is also found in numerous other high-resolution paleoclimate records from the Northern Hemisphere. For instance, several high-resolution North Atlantic Ocean cores have registered a cooling of 1°–2°C around 8 ka [e.g., *Duplessy et al.*, 1992; *Bond et al.*, 1997; *Klitgaard-Kristensen et al.*, 1998]. In addition, records from the European continent indicate cool (0.5°–2°C anomaly) and dry conditions [*Dahl and Nesje*, 1996; *von Grafenstein et al.*, 1998; *Klitgaard-Kristensen et al.*, 1998]. It has been proposed that the 8.2 kyr event is caused by a perturbation of the North Atlantic thermohaline circulation (THC) by a meltwater pulse associated with the final deglaciation stages of the Laurentide ice sheet [*von Grafenstein et al.*, 1998; *Barber et al.*, 1999]. In this paper, we investigate the impact of such freshwater pulses on the early Holocene climate using a coupled three-dimensional climate model.

[3] The effect of changes in the North Atlantic freshwater budget on the stability of the THC has been the subject of numerous climate model studies. These studies suggest that the THC possesses different stable equilibria and that shifts between these states can be triggered by freshwater perturbations [e.g., *Bryan*, 1986; *Marotzke and Willebrand*, 1991; *Rahmstorf*, 1996; *Stocker*, 2000]. For instance, experiments with coupled atmosphere-ocean models have shown that relatively small freshwater releases into the North Atlantic Ocean may result in a temporary century-scale weakening or even shutdown of the THC [e.g., *Stocker and Wright*, 1991; *Manabe and Stouffer*, 1995, 1997; *Fanning and Weaver*, 1997; *Schiller et al.*, 1997]. In these experiments the pattern of surface cooling associated with the THC weakening resembles proxy evidence of past climatic events such as the Younger Dryas (~12.7–11.5 calendar kyr B.P.) [e.g., *Manabe and Stouffer*, 1997; *Mikolajewicz et al.*, 1997]. Besides freshening of the North Atlantic, it has also been suggested that a more vigorous Antarctic Bottom Water circulation could slow down the THC [*Stocker*, 1998; *Seidov et al.*, 2001]. It should be noted that none of the simulations focused at a THC weakening have been started from a climate state in equilibrium with past boundary conditions (e.g., continental ice sheets, insolation, vegetation, and atmospheric greenhouse gas concentrations). Obviously, this hampers the interpretation of freshwater pulse experiments in paleoclimatological terms because it remains unclear what the THC's sensitivity is under past climatic conditions.

[4] In an earlier paper, we presented results of seven numerical experiments performed with a global coupled atmosphere–sea

[1] Now at Faculty of Earth and Life Sciences, Vrije Universiteit Amsterdam, Amsterdam, Netherlands.

0883-8305/02/2001PA000649$12.00

ice–ocean model to study the mechanism behind the 8.2 kyr event [*Renssen et al.*, 2001]. As a first step the model was run with early Holocene (i.e., 8.5 calendar kyr B.P.) boundary conditions until quasi-equilibrium was reached. Subsequently, we perturbed the model's THC by adding realistic freshwater pulses of varying duration (i.e. 10, 20, 50, and 500 years) to the Labrador Sea, while keeping the total amount of freshwater released fixed at 4.67×10^{14} m^3. In one particular scenario, with freshwater released at a rate of 0.75 Sv (1 Sv = 10^6 m^3 s^{-1}) during 20 years, the model simulated a cooling event that was similar in magnitude and duration to what is found in proxy records. We concluded that this result supports the hypothesis that the 8.2 kyr event was caused by a meltwater-induced THC perturbation. It was also found that the timescale of the freshwater release and the initial state (i.e., natural climate variability) are important, as both have a strong effect on the magnitude and duration of the produced model response [*Renssen et al.*, 2001].

[5] In the present paper, we extend our study of the effect of meltwater pulses on the early Holocene climate, thereby further investigating the importance of the natural climate variability. It is well known from climate model studies on seasonal-to-annual timescales that initial conditions can have a strong effect on the outcome [e.g., *Brankovic et al.*, 1994; *Anderson and Ploshay*, 2000]. If, for example, a global atmospheric model is run several times with minimal changes in the initial state but with identical boundary conditions (i.e., ensemble experiments), significant differences between the final solutions of the individual ensembles are found. In other words, atmospheric dynamics are known to be very sensitive to natural climate variability on relatively short timescales. The effect of this variability on a longer (decadal to millennial) timescale has not been studied yet thoroughly in ensemble experiments with fully coupled atmosphere-ocean general circulation models (GCMs), as these models are extremely expensive to run. Nevertheless, the strong sensitivity of the THC in these models to various kinds of relatively small changes (e.g., in diffusion parameters or freshwater budget) suggests that initial conditions may have a strong impact on longer timescales [e.g., *Tziperman*, 1997, 2000a, 2000b; *Manabe and Stouffer*, 1999]. Furthermore, *Knutti and Stocker* [2002] have shown with a simplified climate model that the response of the THC to future anthropogenic warming may be unpredictable due to a strong dependence on initial conditions. Because of a simplified three-dimensional atmospheric component, our model is much faster than coupled GCMs, making the performance of ensemble runs of several hundred years feasible. Therefore, to study the impact of the high-frequency variability in the atmosphere–sea ice–ocean system in our THC perturbation experiments, we have performed in total five ensemble experiments for each of the 10, 20, and 50 year perturbation cases. These ensemble simulations are initialized with different samples from the same quasi-equilibrium (early Holocene) climate. We compare our results with proxy evidence, thereby focusing on the Northern Hemisphere.

2. Model

[6] The numerical experiments were performed with ECBilt-CLIO, a three-dimensional atmosphere–sea ice–ocean model. The atmospheric component is version 2 of ECBilt, a spectral T21, three-level, quasi-geostrophic model set up at the Koninklijk Nederlands Meteorologisch Instituut (KNMI), de Bilt [*Opsteegh et al.*, 1998]. This model includes a representation of the hydrological cycle and simple parameterizations of the diabatic heating processes. Cloudiness is prescribed according to present-day climatology. The model has a dynamically passive stratospheric layer. As an extension to the quasi-geostrophic equations, an estimate of the neglected terms in the vorticity and thermodynamic equations is incorporated as a temporally and spatially varying forcing. This forcing is computed from the diagnostically derived vertical motion field. With the inclusion of the ageostrophic terms the simulation of the Hadley circulation is considerably improved. This, in turn, results in a drastic improvement of the strength and position of the jet stream and transient eddy activity. The hydrological cycle is closed over land by using a bucket for soil moisture. Each bucket is connected to a nearby oceanic grid cell to define river runoff. Accumulation of snow occurs in case of precipitation in areas with below 0°C surface temperature.

[7] The sea ice–ocean component is the CLIO model built at Université catholique de Louvain, Louvan-la-Neuve [*Goosse and Fichefet*, 1999]. This model is made up of a primitive-equation, free surface ocean general circulation model (OGCM) [*Deleersnijder and Campin*, 1995; *Campin and Goosse*, 1999] coupled to a comprehensive thermodynamic-dynamic sea ice model [*Fichefet and Morales Maqueda*, 1997]. The OGCM contains a detailed formulation of boundary layer mixing based on *Mellor and Yamada*'s [1982] level 2.5 turbulence closure scheme [*Goosse et al.*, 1999] and a parameterization of density-driven downslope flows [*Campin and Goosse*, 1999]. The horizontal eddy diffusivity and viscosity in the ocean are set equal to 300 and 10^5 m^2 s^{-1}, respectively. Real freshwater fluxes are applied at the ocean surface [*Tartinville et al.*, 2001]. The sea ice model takes into account the heat capacity of the snow-ice system, the storage of latent heat in brine pockets trapped inside the ice, the effect of the subgrid-scale snow and ice thickness distributions on sea ice thermodynamics, the formation of snow ice under excessive snow loading, and the existence of leads within the ice cover. Ice dynamics are calculated by assuming that sea ice behaves as a two-dimensional viscous-plastic continuum. The horizontal resolution of CLIO is $3° \times 3°$, and there are 20 unequally spaced vertical levels in the ocean. Special software (named OASIS; see *Terray et al.* [1998] for details) ensures a synchronous coupling (every 24 hours) of ECBilt and CLIO and performs the spatial interpolation of the coupling fields from one grid to the other. The atmospheric and oceanic components run with time steps of 4 and 24 hours, respectively.

[8] Under present-day forcing conditions, ECBilt-CLIO systematically overestimates the freshwater input into the North Atlantic and Arctic Oceans [*Opsteegh et al.*, 1998]. The immediate consequence is a too slow THC and an erroneous mass balance of the Arctic snow-sea ice pack. To overcome this problem, we artificially reduce (in all experiments) precipitation by 10% over the Atlantic basin and by 50% over the Arctic Ocean and distribute this excess water homogeneously over the Pacific Ocean, where the simulated precipitation is generally too weak [*Goosse et al.*, 2001]. With this sole flux correction, the model reproduces the main characteristics of present-day climate. As already mentioned, the main advantage of ECBilt-CLIO compared to fully coupled GCMs is that it is much faster. This makes it feasible to study the behavior of the coupled atmosphere–sea ice–ocean system on a multicentennial timescale, without the burden of requiring powerful computing facilities. With ECBilt-CLIO, a run of 1000 years takes ~25 days CPU time on a standard workstation (i.e., Hewlett Packard S-Class 4CPU/1 GB RAM). It should be realized, however, that ECBilt-CLIO represents a simplified description of the climate system compared to coupled GCMs. This is especially true for the atmospheric component ECBilt, as it is based on quasi-geostrophic equations, making it less suitable for the simulation of low-latitude atmospheric dynamics. Accordingly, the model results for the tropics should be treated with caution. Moreover, its resolution is relatively low (~5.6° latitude-longitude), so that, for instance, it is not possible to resolve features related to regional orography. However, it should be noted that the three-dimensional description of the coupled atmosphere–sea ice–ocean system in ECBilt-CLIO is much more comprehensive than the two-

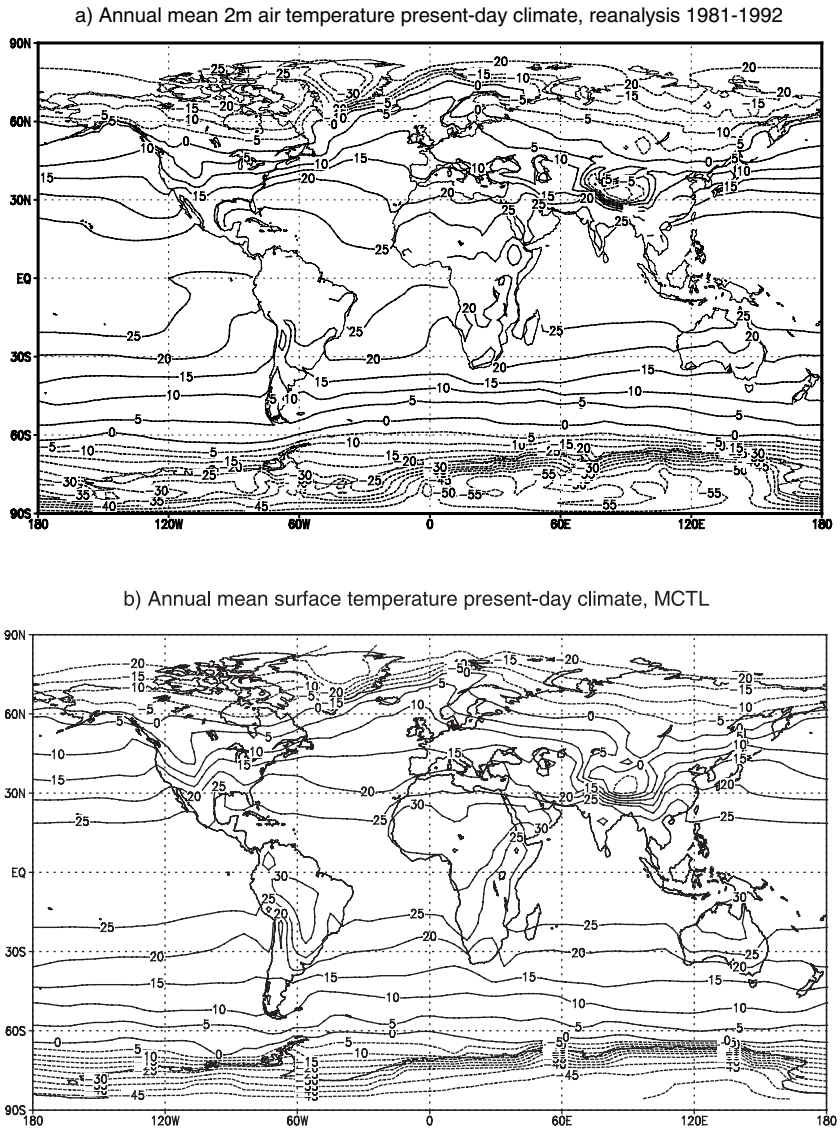

Figure 1. Annual mean surface temperatures. (a) DAO (Data Assimilation Office) reanalyses for 1981–1992 [*Schubert et al.*, 1993]; (b) MCTL. Contour interval is 5°C.

dimensional representation in most other so-called Earth system models of intermediate complexity (EMICs) [e.g., *Petoukhov et al.*, 2000; *Wang and Mysak*, 2000; *Claussen et al.*, 2002; *Crucifix et al.*, 2002]. In addition, in contrast to other EMICs, our model has an atmospheric component that simulates atmospheric weather patterns.

3. Simulated Modern and Early Holocene Climates

3.1. Modern Climate

[9] The present-day climate was simulated in a transient experiment starting from a climate state in equilibrium with preindustrial (i.e., 1750 A.D.) values of greenhouse gas concentrations. Subsequently, the model was run for 250 years with annually increasing greenhouse gas concentrations (i.e., until 2000 A.D.). This procedure was chosen because it was recently shown that modern climate is not in equilibrium with present-day boundary conditions due to the long time-scale memory of the deep ocean [e.g., *Weaver et al.*, 2000; *Goosse and Renssen*, 2001]. The average over 1950–2000 is taken here as the modern control climate (hereafter MCTL). A comparison between the simulated annual mean temperatures and those derived from reanalysis data for the period 1981–1992 shows general agreement (see Figures 1a and 1b). However, the model generates a too weak east-west thermal gradient in the tropics, resulting in too high temperatures in the east Pacific. In the tropics, ECBilt-CLIO also underestimates precipitation (Figures 2a and 2b). The model's bias in the low latitudes is a direct consequence of the quasi-geostrophic equations in ECBilt, which hamper a correct simulation of the Hadley circulation. In the extratropics the model gives a fair representation of the main features of precipitation, despite the too weak midlatitude storm tracks. The simulated pattern of atmospheric circulation in the Northern Hemisphere middle to high latitudes is comparable to reanalysis data, with similar positions of the Icelandic and Aleutian Lows [*Goosse et al.*, 2001]. This warrants realistic wind directions over the North Atlantic and Pacific Oceans. However, in the model, the meri-

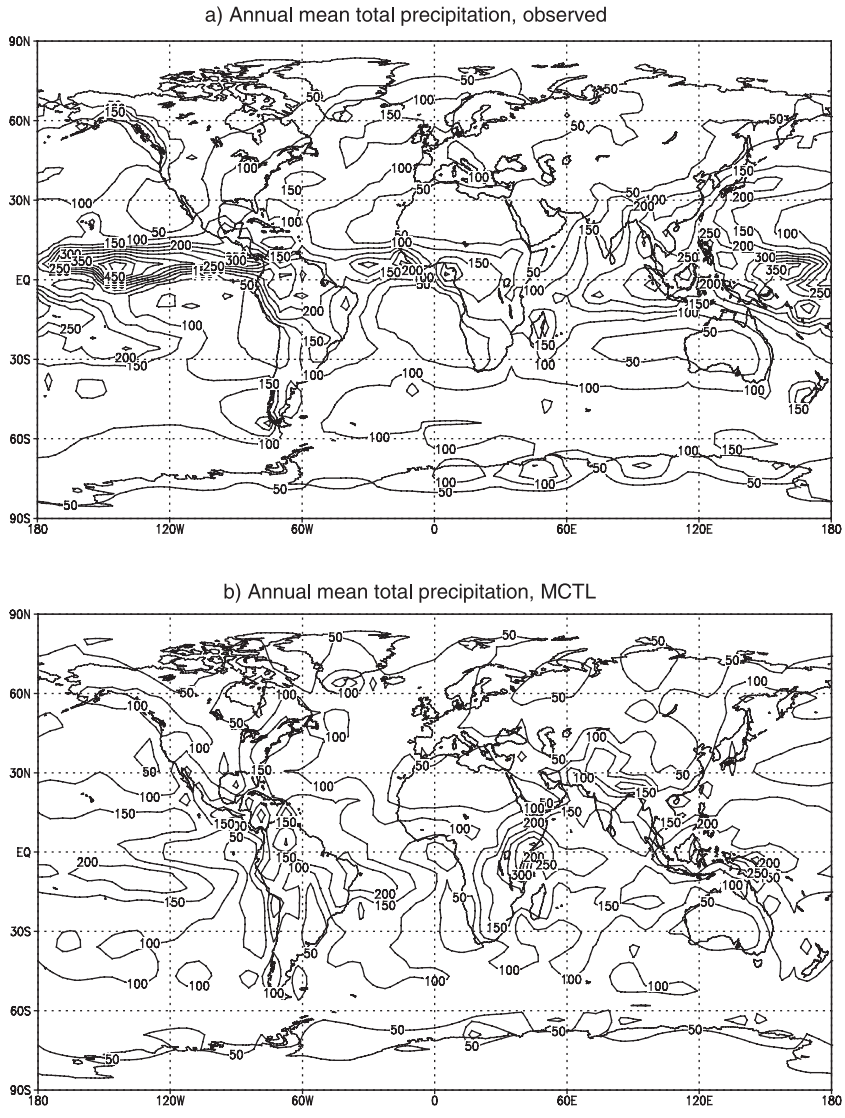

Figure 2. Annual mean precipitation. (a) Observed [*Legates and Willmott*, 1990] and (b) MCTL. Contour interval is 50 cm yr^{-1}.

dional gradient of geopotential height is underestimated over the Atlantic, whereas the Aleutian Low has a too large extension.

[10] In the ocean, the model produces a circulation that falls within estimates for the modern climate (Figure 3) [see, e.g., *Schmitz*, 1995]. In the Atlantic Ocean, North Atlantic Deep Water (NADW) overturning with a maximum rate of 19 Sv is generated, with 14 Sv being exported at 20°S, whereas the maximum Antarctic Bottom Water (AABW) inflow is 6 Sv, and its waters reach 50°N (Figure 3). NADW is formed mainly between 70° and 80°N (i.e., in the Nordic Seas). Consequently, in contrast to observations, the model simulates no deep convection in the Labrador Sea. In the Indo-Pacific basin, total equatorial upwelling amounts to 38 Sv, whereas the global meridional stream function shows a clockwise cell near Antarctica with a maximum flow of 24 Sv (not shown).

[11] The sea ice model generates in both hemispheres a sea ice distribution that is in reasonable agreement with modern observations. For example, the simulated location of the Northern Hemisphere sea ice edge (Figures 4a and 4b) is comparable to that observed by *Gloersen et al.* [1992] for both winter and summer, except for the Barents Sea where the model underestimates the sea ice concentration throughout the year. In addition, in the Northern Hemisphere the sea ice area in MCTL ranges from 6.7×10^{12} km^2 in summer to 14.5×10^{12} km^2 in winter, while the observed values are 6.2 and 13.9×10^{12} km^2, respectively [*Gloersen et al.*, 1992]. In the Southern Hemisphere the simulated values are 2.2×10^{12} km^2 in summer and 11.5×10^{12} km^2 in winter, while the observations suggest 2.2 and 15.2×10^{12} km^2, respectively [*Gloersen et al.*, 1992].

3.2. Early Holocene Climate

[12] To simulate the climate of 8.5 calendar kyr B.P., several boundary conditions were altered compared to the modern control experiment. Insolation was changed to 8.5 calendar kyr B.P. values following *Berger* [1978], with higher values in July (e.g., +41 W m^{-2} at 65°N) and lower values in January (e.g., −21 W m^{-2} at 65°N). Atmospheric concentrations of greenhouse gases were lowered from their modern values in agreement with

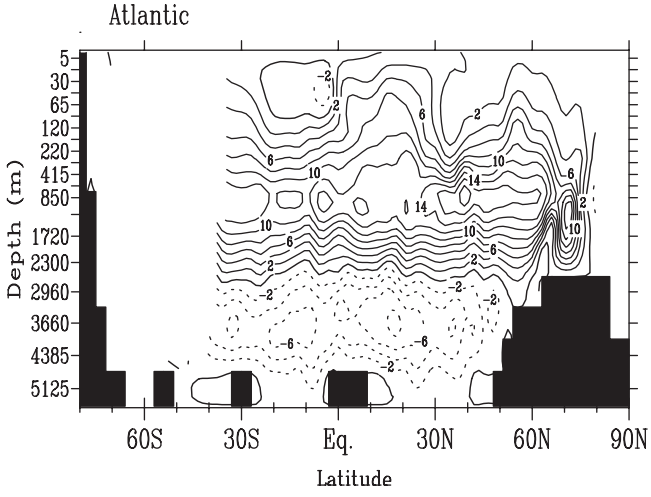

Figure 3. Latitude-depth distribution of the annual mean meridional overturning stream function in the Atlantic Ocean for MCTL. Contour interval is 2 Sv. The flow is clockwise around solid contours.

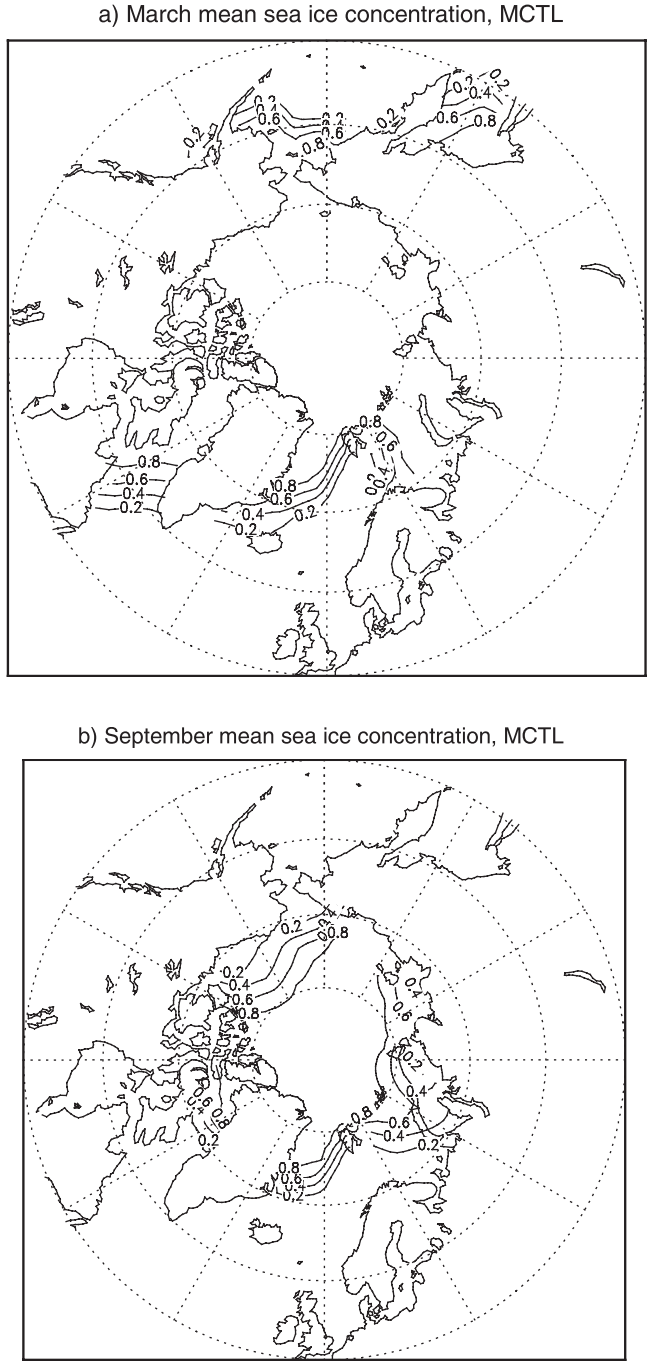

Figure 4. Mean sea ice concentration (fraction) in MCTL. (a) March and (b) September. Contour interval is 0.2.

ice core analyses (i.e., CO_2 from 353 to 261 ppmv, CH_4 from 1720 to 650 ppbv, and N_2O from 310 to 270 ppbv [*Raynaud et al.*, 2000]). In addition, the surface albedo was altered to account for global vegetation changes, following the reconstruction of *Adams and Faure* [1997]. The latter modification involves important lowering of the surface albedo in North Africa (change from desert to savanna) and Europe (change from agricultural fields to closed forest). Moreover, for some grid cells on the North American continent the surface albedo was adjusted, and the elevation was increased to account for the remnant of the Laurentide ice sheet (assuming a deglaciated Hudson Bay) [*Peltier*, 1994]. Starting from a modern quasi-equilibrium climate state, the model was run with these 8.5 ka boundary conditions until it reached a new quasi-equilibrium after 500 years. Subsequently, the run was continued for another 50 years (until t = 550 years). The results of the years 500–550 are used in this paper to analyze the 8.5 ka early Holocene quasi-equilibrium state (hereafter called HCTL). In this state the trend of the global mean ocean temperature is only −0.007°C per century.

[13] Compared to MCTL, the first evident difference in HCTL is the increased seasonality due to orbital forcing (see Figures 5a and 5b). In boreal summer (June–July–August (JJA)) the surface temperatures over most continents are 1°–5°C higher in HCTL than in MCTL. In boreal winter (December–January–February (DJF)) they are generally lower (1°–2°C) over low- and middle-latitude continents, except for North Africa. The larger JJA anomaly is consistent with the prescribed orbital forcing. At high latitudes a clear positive temperature anomaly is present in both seasons, especially in the winter hemisphere, where it amounts to >2°C. These warm conditions in winter are due to a strong reduction of the sea ice thickness (by 0.5–3 m, not shown) that is associated with the summer insolation maximum, reducing the insulating effect of sea ice. Over middle- and high-latitude oceans, the simulated HCTL-MCTL temperature anomaly is small, mostly below 1°C. At a regional level the effect of the prescribed albedo changes is visible, for instance, as a negative temperature anomaly in the Hudson Bay region (ice sheet) and higher HCTL temperatures in North Africa and Europe (vegetation). A marked positive HCTL-MCTL precipitation anomaly of up to 50 cm yr^{-1} is simulated over North Africa, Arabia, and central Asia (Figure 6). This positive anomaly is associated with the relatively strong warming over these land surfaces compared to the surrounding oceans, producing a strengthening of the summer monsoon circulation.

[14] In HCTL the Atlantic Ocean circulation is very similar to MCTL, with 12 Sv of NADW exported at 20°C (compare Figures 3 and 7). The same is true for the overturning circulation in the Indo-Pacific and Southern Oceans (not shown). The largest HCTL-MCTL difference in sea ice concerns the mentioned strong reduction in ice thickness in both hemispheres. In the Arctic region

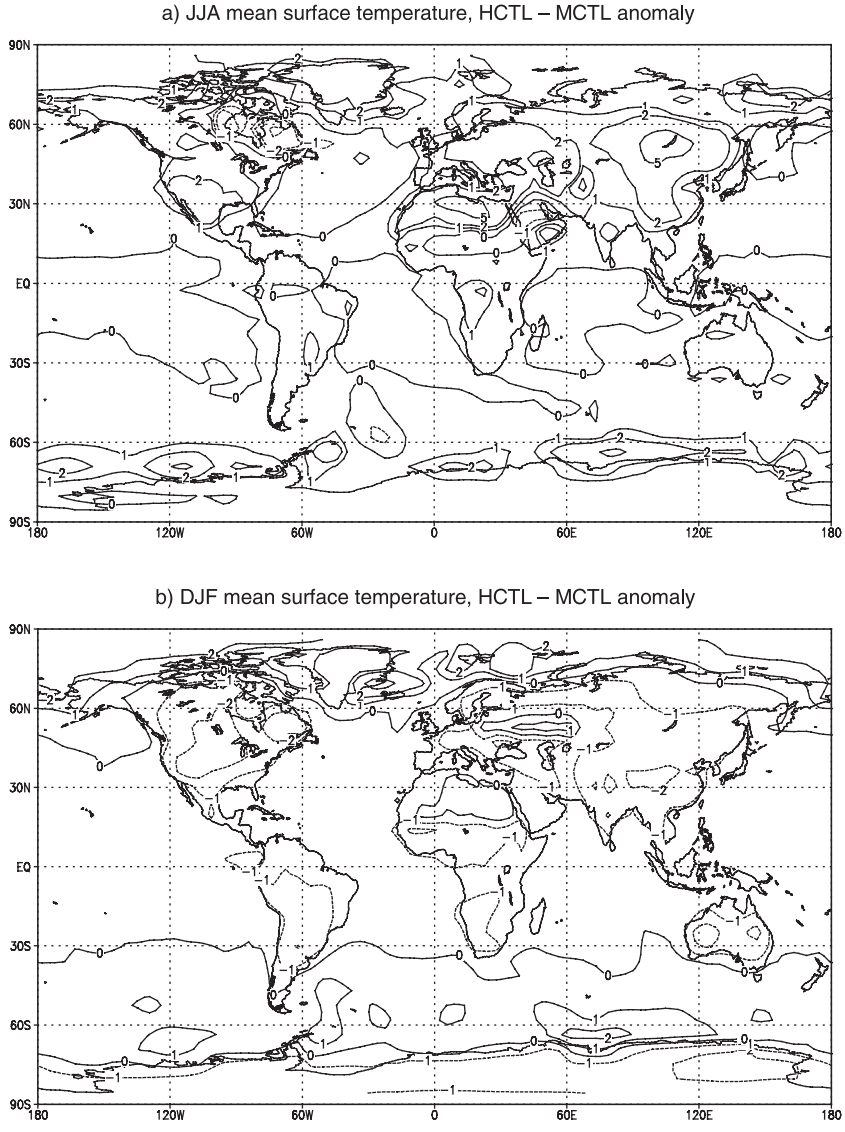

Figure 5. Seasonal mean surface temperature HCTL-MCTL anomalies. (a) June–July–August (JJA), and (b) December–January–February (DJF). Contours are at −5°, −2°, −1°, 0°, 1°, 2°, and 5°C.

the ice thickness is reduced by up to 3 m, whereas near Antarctica the decrease amounts to 1 m in the Weddell Sea (not shown). By contrast, the changes in sea ice areal coverage in HCTL compared to MCTL are relatively modest [see *Renssen et al.*, 2001].

[15] Our HCTL results are consistent with earlier experiments performed with atmospheric GCMs coupled to mixed layer ocean models to study the impact of orbital forcing at 9 kyr B.P. [*Kutzbach and Gallimore*, 1988; *Mitchell et al.*, 1988]. These simulations show, compared to a modern control experiment, higher JJA temperatures and lower DJF values over middle- and low-latitude continents, with a difference of up to 2°–4°C in both seasons. Moreover, in these experiments, a high-latitude warming and a reduction in sea ice thickness are also present as well as a precipitation increase at low latitudes.

[16] The simulated early Holocene climate is in general agreement with proxy data. The simulated warm conditions over the Northern Hemisphere continents are coherent with the reconstructed early Holocene tree line limit in northern Eurasia, which was positioned a few hundred kilometers to the north compared to today [*MacDonald et al.*, 2000]. In addition, evidence from cores from the North Atlantic Ocean and the Nordic Seas suggests that at high latitudes the positive temperature anomaly compared to today was larger (2°–5°C) than at middle and low latitudes (generally <2°C, except in upwelling regions [see, e.g., *Koç et al.*, 1993, *Koç et al.*, 1996; *Koç and Jansen*, 1994; *Schulz*, 1995]). This is in agreement with the simulated strong meridional gradient in sea surface temperatures (SSTs) and relatively thin sea ice in the Arctic. Reconstructions from Greenland ice cores suggest also higher temperatures (∼2°C) for the early Holocene compared to modern climate [*Cuffey et al.*, 1995]. Antarctic ice cores show temperatures that are 0.2°–2.5°C higher (depending on the site) for the early Holocene than today [*Masson et al.*, 2000]. Moreover, the clear positive precipitation HCTL-MCTL anomaly in North Africa is consistent with the high lake levels reconstructed for the early Holocene [e.g., *Gasse and Van Campo*, 1994]. According to *Hillaire-Marcel et al.* [2001], deep water information in the Labrador Sea was absent during the early Holocene (as in all our model states), as this started ∼7000 ^{14}C years B.P. To our knowl-

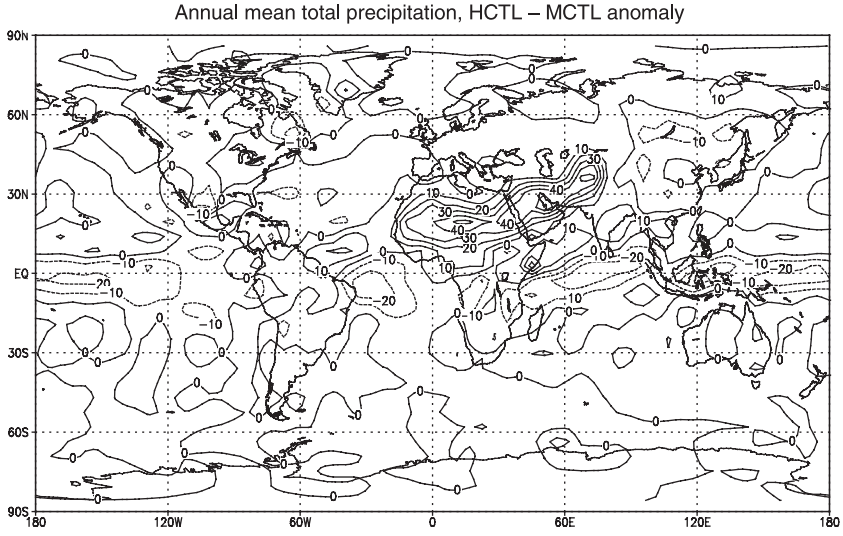

Figure 6. Annual mean total precipitation HCTL-MCTL anomaly. Contour interval is 10 cm yr^{-1}.

edge, no further indications for changes in deep ocean circulation during the early Holocene have been inferred from marine proxy data [e.g., *Veum et al.*, 1992; *Charles and Fairbanks*, 1992].

4. Freshwater Perturbation Experiments

[17] As a second step, we perturbed the 8.5 kyr quasi-equilibrium state in a series of experiments. In these experiments the amount of freshwater released was kept fixed at 4.67×10^{14} m^3, which is close to the highest estimate for the 8.2 kyr event based on geological data (i.e., 5×10^{14} m^3 [*von Grafenstein et al.*, 1998]). This fixed amount of freshwater was released into the Labrador Sea at three different constant rates: (1) 1.5 Sv during 10 years, (2) 0.75 Sv during 20 years, and (3) 0.3 Sv during 50 years. The 10, 20, and 50 year cases were performed five times, each with different initial conditions, which were obtained by taking samples from a continuation of the early Holocene quasi-equilibrium experiment (from year 550 to 570). An arbitrary interval of 5 years was chosen between the different samples. Consequently, our ensemble perturbation experiments started at years 550, 555, 560, 565, and 570. The five ensembles have been labeled with "a" to "e" (e.g., a = 550, b = 555, etc.). In an earlier work [*Renssen et al.*, 2001], we reported on the results of the perturbation experiments with start times of 550 and 555 and also on an additional experiment in which 0.03 Sv was released during 500 years.

4.1. THC Response to Freshwater Pulses

[18] As expected, the surface freshening produces a weakening of the THC. As reported by *Renssen et al.* [2001], the THC is only very slightly weakened with a pulse of 500 years, with a maximum strength of meridional overturning in the Nordic seas of 16 Sv instead of 17 Sv. In the other cases, both duration and timing of freshwater pulses influence the model's THC response (see Figures 8a–8c). In the five 50 year cases the model shows similar responses. During these perturbations the maximum meridional overturning in the Nordic Seas gradually weakens until the end of the pulse (from 17 to 4–7 Sv), after which the overturning recovers gradually to its preperturbed level within 120–200 years (Figure 8a). In the 10 and 20 year cases the model response is less straightforward (Figures 8b and 8c). In some instances, the overturning in the Nordic seas recovers at a similar timescale as in the 50 year cases, i.e., in two 20 year experiments (c and e) and one 10 year case (d). With other initial conditions, however, the model's THC shifts toward a new quasi-equilibrium that is characterized by a reduction in meridional overturning and a higher variability. This quasi-equilibrium is marginally stable, as is evidenced by three examples of recovery from this state. In one example, the model's THC recovers from a 20 year perturbation after 320 years (case a in Figure 8b). In the other examples the meridional overturning stays in the perturbed mode for >1200 years, after which the THC returns to its preperturbed mode in two cases (case b in Figure 8b, recovery after 1280 years, and case a in Figure 8c, recovery after 1270 years). However, in the 20 year case, d (Figure 8b), the THC does not recover within 1400 years after the perturbation. The latter experiment and the other cases without recovery have not been continued to avoid high computational costs. In conclusion, we have recognized two types of THC recovery that differ in timescale: (1) on a

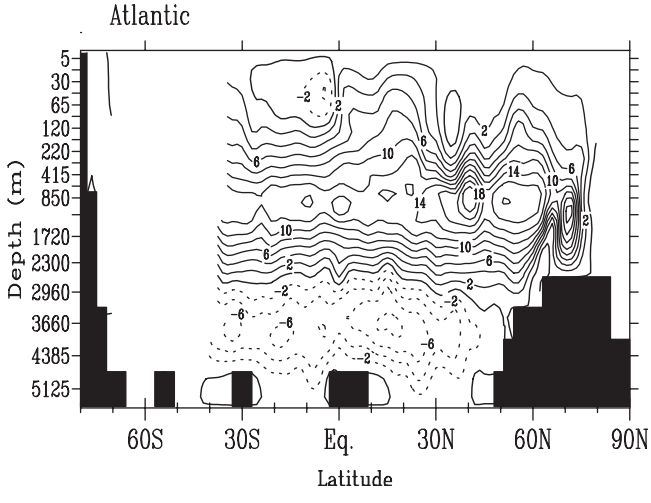

Figure 7. Latitude-depth distribution of the annual mean meridional overturning stream function in the Atlantic Ocean for HCTL. Contour interval is 2 Sv. The flow is clockwise around solid contours.

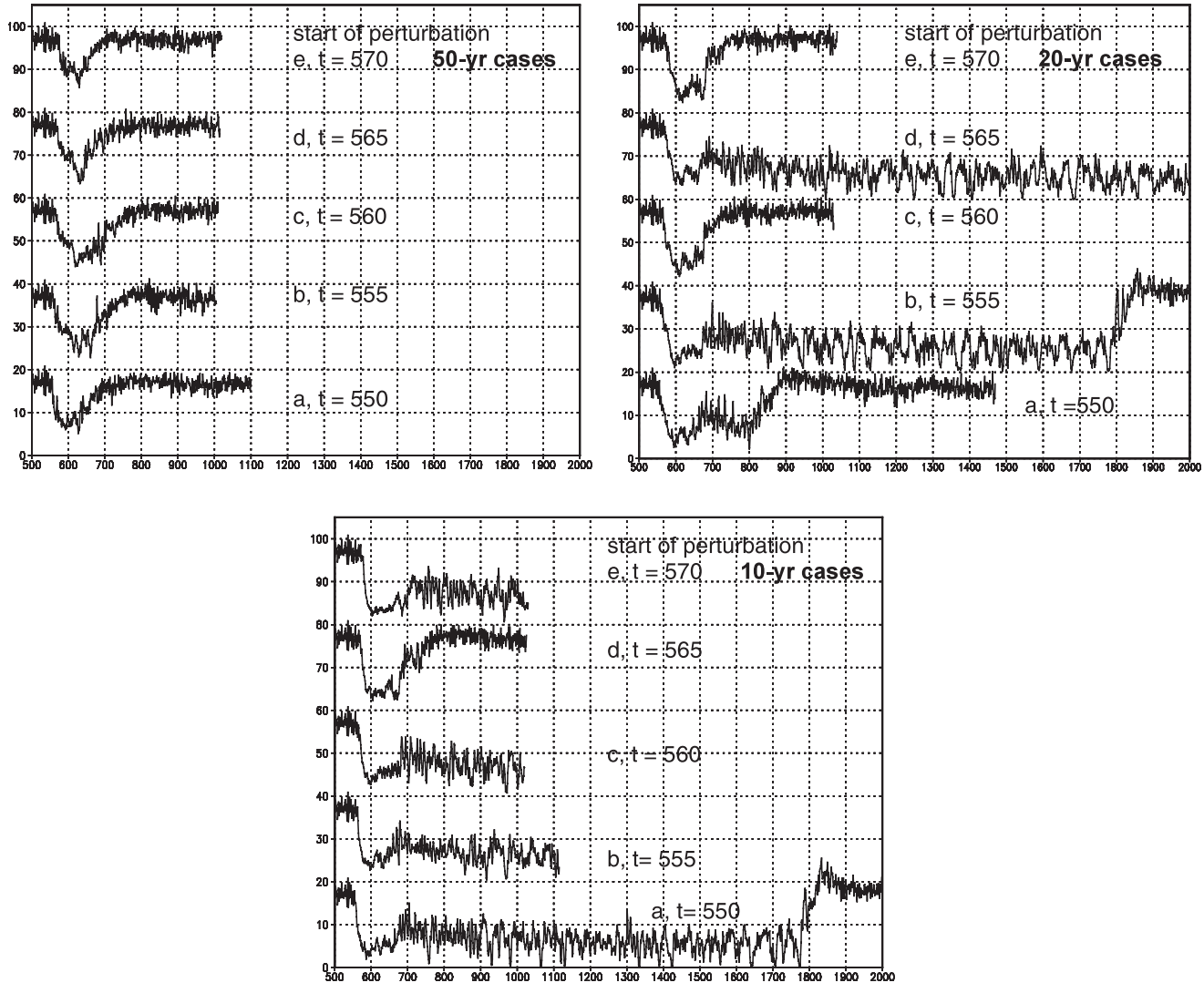

Figure 8. Maximum meridional overturning rate (Sv) in the Nordic seas (i.e., between 60° and 80°N) plotted against time (years) for all ensemble experiments. (a) The 50 year cases, (b) 20 year cases, and (c) 10 year cases. The start times of the ensembles (labeled "a" to "e") are indicated. Note that, for convenience, values of the upper top curves have been elevated by 20, 40, 60, and 80 Sv.

relatively short timescale ($\leq$200 years) and (2) on a long timescale (>200 years).

[19] The type of recovery is not simply a linear function of the duration of the freshwater pulse. This complexity is depicted in Figure 9, in which the recovery time is plotted for all perturbation experiments. Figure 9 shows that the timescale of the perturbation is important, as in all 50 year cases the model recovers within 200 years (i.e., type 1). However, the variation in the recovery times for the 20 and 10 year cases indicates that the type of recovery follows a statistical probability function, with a recovery of type 2 becoming more likely when the duration of the freshwater pulse becomes shorter. Hence there is also a chance that a 50 year pulse could produce a THC recovery on a longer timescale than 200 years. The nonlinearity of the THC recovery is illustrated by the model response in the perturbation experiments started with initial state d. In the 10 year case the model responds with a short timescale recovery, whereas in the 20 year case the model's THC is not recovering within 500 years. Thus the type of recovery is not related to a particular characteristic of the initial state that could be identified. Consequently, we can conclude that the type of recovery is unpredictable in the model states studied here. The only physical information that could be obtained is the probability of each type of recovery, which could only be determined by performing a very large number of experiments. This is, however, with our model and available resources at present not feasible. Moreover, as the computed probability is most likely dependent on the amount of freshwater and on the model used, it is questionable if this probability function would have a general applicability.

[20] We propose that the unpredictability of the THC recovery is due to its link with high-frequency climate variability. Considering this high-frequency variability in the meridional overturning plots (Figures 8a–8c), it is evident that it is relatively weak during the first $\sim$100 years of the THC weakening. This small variability is related to the presence of the fresh surface water layer in the Nordic seas region, which suppresses most deep convection. After some time, meridional overturning is increasing again, thereby showing a kind of overshoot behavior around year 650–680 (Figures 8a–8c). It appears that in the 20 and 10 year cases the amplitude of this

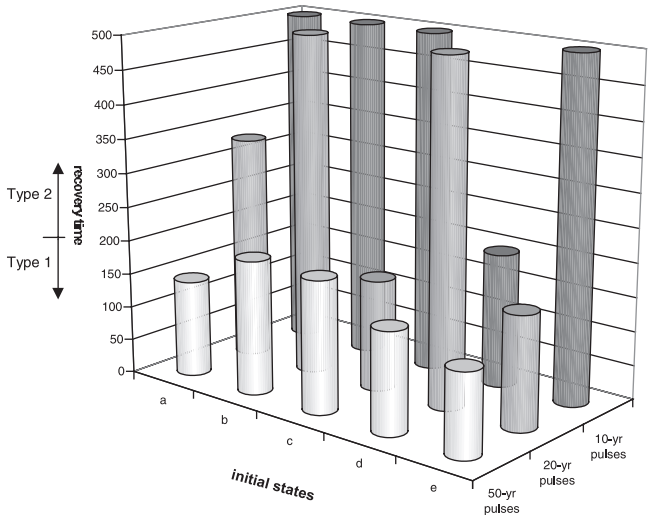

Figure 9. Recovery time (in years after start of perturbation) of meridional overturning in the Nordic seas plotted for all perturbation experiments. The end time of the simulated perturbation events is defined as the year when the meridional overturning has reached the annual mean level of HCTL (17.2 Sv). Note that a recovery time of 500 years should be read as >500 years.

increase plays an important role in determining the type of recovery of the model's THC (i.e., type 1 or 2). If the increase is relatively strong, the THC shifts to the preperturbed mode of HCTL, with deep convection just south of Svalbard (centered at 74°N, 13°E). If, on the other hand, the increase is relatively weak, the model's THC stays in the weakened mode with deep convection at a more southward location near the Norwegian coast (66°N, 5°E; see *Renssen et al.* [2001] and Figure 10). Comparable shifts between convection sites have been described in earlier model studies [see, e.g., *Lenderink and Haarsma*, 1994; *Rahmstorf*, 1995]. The weakened THC state is further characterized by a reduction in NADW export at 20°S from 13 Sv in HCTL to 10 Sv (Figure 10). The NADW cell also becomes shallower at the expense of the AABW cell. The latter expands also latitudinally and reaches up to 60°N (HCTL: 50°N).

[21] The weakened overturning mode is further characterized by a stronger variability on a decadal timescale. The maximum meridional overturning rate in the Nordic seas fluctuates between 0 and 10 Sv, whereas in HCTL these values are ~15 and 20 Sv (Figures 8a–8c). These fluctuations are coherent with variations in sea ice cover, sea surface salinity (SSS), sea surface temperature (SST), and convective activity. This coherent structure is illustrated in Figures 11a–11c, showing an example (20 years (a)) of time series of SSS and convective activity for three grid points in the Nordic seas. At the main convection site in HCTL (74°N, 13°E, Figure 11a), deep convection stops after year 580, but SSS shows strong variations at an annual-to-decadal timescale (duration of cycles is 7–11 years). To the south, between the two discussed convection sites (i.e., at 71°N, 8°E and 71°N, 0°E), the convective activity fluctuates coherently with these SSS variations (Figures 11b and 11c). In simulations of modern climate with the same model, variations at a similar decadal timescale occur in the Nordic seas region. As discussed in detail by *Goosse et al.* [2002], the decadal variability in the Nordic seas region can be explained by a complex feedback loop, involving all components of the atmosphere-sea ice-ocean system (see *Goosse et al.* [2002] for details). In the particular case illustrated in Figures 11b and 11c, recovery of the THC (i.e., of type 2) appears to be related to the strong decadal variability, more particular with a large positive anomaly in SSS in year 820. This SSS anomaly is accompanied by deep convection at 71°N (Figures 11b and 11c), but also at the main location of convection in HCTL (i.e., at 74°N, 13°E, Figure 11a). After year 820, the model's THC shifts to the preperturbed mode in the 20 year (a) perturbation experiment. The same connection between decadal variability and recovery is seen in the other type 2 cases that have been continued until recovery (20 year case (b) and 10 year case (a)). It is thus conceivable that the stability of the weakened mode is intimately linked to this high-frequency variability. This would imply that the moment of recovery of the type 2 cases is also unpredictable because it depends on the magnitude of decadal variability in the system.

4.2. Surface Climate of Perturbed State

[22] A clear reduction in surface temperature is associated with the perturbed climate state (i.e., first 50 years of 20 year (a) perturbation, see Figures 12a and 12b). In DJF this reduction exceeds 10°C in the Nordic seas region, where the main convection site of HCTL is now perennially covered by sea ice [*Renssen et al.*, 2001]. The annual mean sea ice volume in the Northern Hemisphere increases from 16×10^3 km^3 to 23×10^3 km^3. Over the Arctic Ocean the DJF temperature lowering is between 5° and 10°C, whereas it varies from 0.5° to 5°C over adjacent land surfaces (Figure 12b). In JJA the reduction is generally less pronounced, except over the North Atlantic and Europe where the temperature lowering is of the same order as in DJF (i.e., 0.5°–2°C; Figure 12a). No clear response in temperature is seen in the tropics and the Southern Hemisphere. This is different for precipitation, which is reduced by up to 10 cm yr^{-1} over North Africa, the Middle East, and southern Europe (Figure 13). A clear reduction is also visible over southeast Greenland (−30 cm yr^{-1}) and over the Nordic seas near Svalbard. In contrast, precipitation increases over northern Scandinavia.

[23] The precipitation changes are associated with modifications in atmospheric circulation that are mostly related to the increase in meridional temperature gradient. This enhanced gradient generates an intensification of the atmospheric circulation

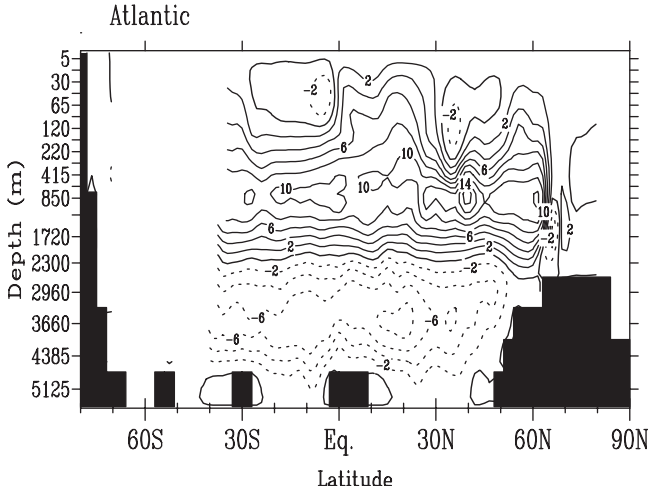

Figure 10. Latitude-depth distribution of the annual mean meridional overturning stream function for the perturbed state in the Atlantic Ocean. Here the example of 10 year case (e) is given. Contour interval is 2 Sv. The flow is clockwise around solid contours.

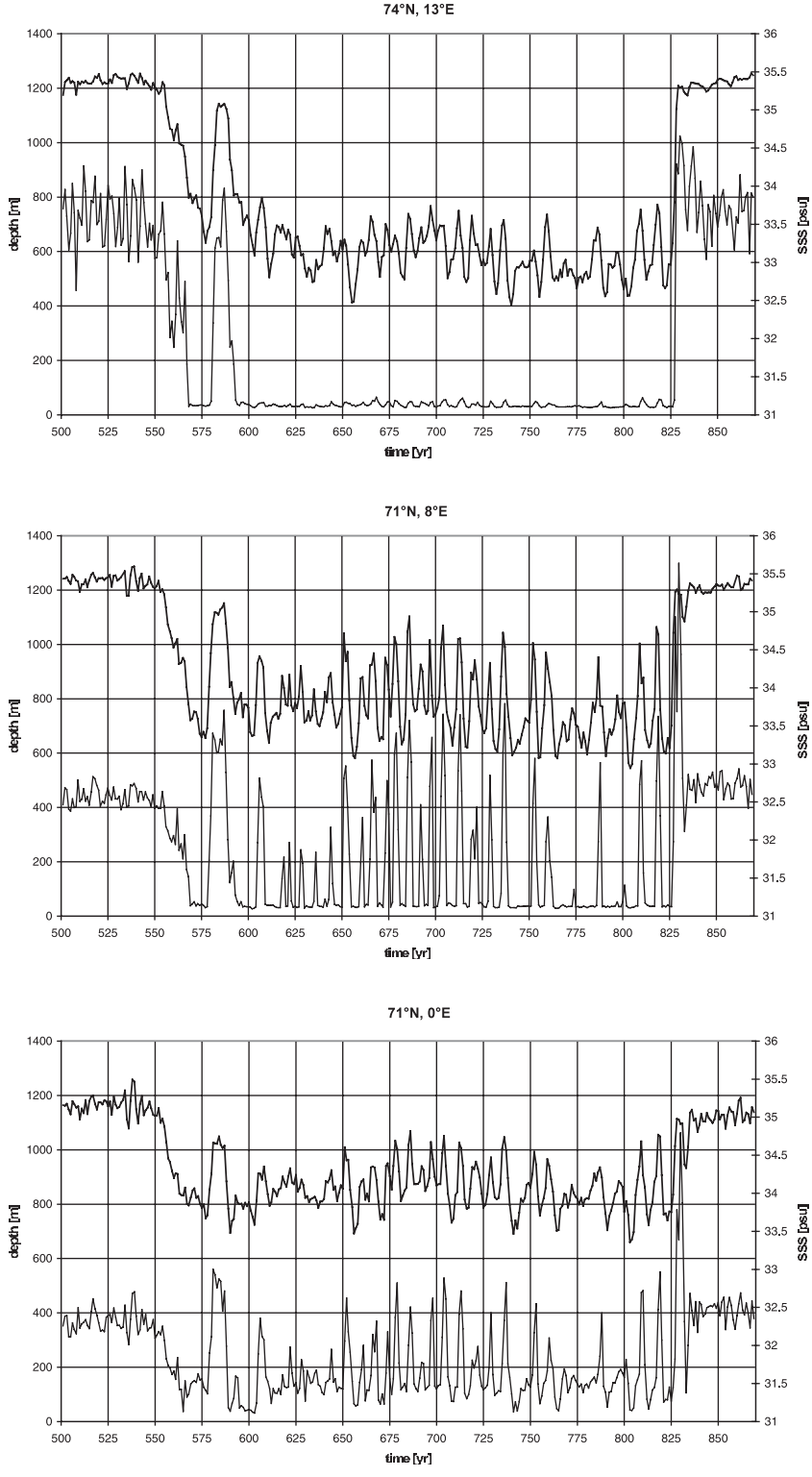

Figure 11. Time evolution for 20 year (a) perturbation experiment of sea surface salinity (top curves, right axis in psu) and maximum convection depth (bottom curves, left axis in m) at three grid point in the Nordic Seas: (a) 74°N, 13°E, main convection site preperturbed state; (b) 71°N, 8°E; and (c) 71°N, 0°E.

and an increase in wind speed in most places (see Figure 14). An exception is the reduction in wind speed over the Nordic seas and the adjacent part of the Arctic Ocean. The latter reduction in wind speed is associated with strong cooling over the perennially sea ice covered surface, inducing a relatively high atmospheric surface pressure there (anomaly of 25 hPa; Figure 15a). This high pressure implies stabilization of the atmosphere in this region, thus blocking depressions that now take a more southerly route

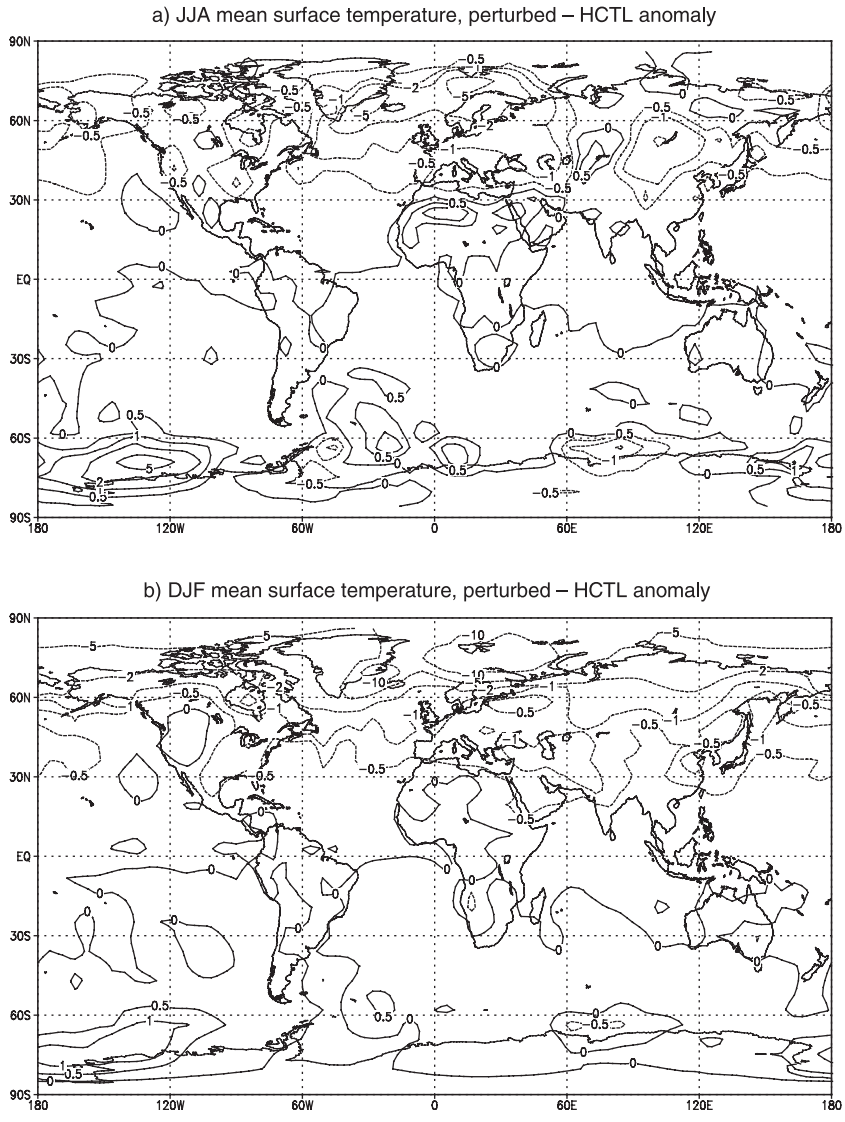

Figure 12. Seasonal mean surface temperature anomalies (20 year (a) perturbation, HCTL). (a) JJA and (b) DJF. Contours at −10°, −5°, −2°, −1°, −0.5°, 0°, 0.5°, 1°, 2°, 5°, and 10°C.

over Europe (increasing wind speed at 55°N). The noted change in atmospheric circulation has also implications for sea ice transport in the Nordic seas region. The anticyclonic circulation anomaly centered near Svalbard causes an increase in sea ice transport from the Barents Sea to the site of convection. The latter transport is very weak in HCTL (Figures 15b and 15c). This enhanced sea ice influx from the Barents Sea represents a considerable increase in the freshwater transport to the site where convection takes place in HCTL, thus increasing the stabilization of the water column. Consequently, a positive feedback exists between ocean circulation, sea ice, and atmosphere that stabilizes the perturbed state. To our knowledge, this feedback has not been described before.

4.3. Comparison of Surface Climate With Proxy Data

[24] To establish if the simulated changes are realistic, it is important to compare our experimental results with proxy evidence for the 8.2 kyr event (see Figure 16). This comparison reveals a general agreement. The 3°–8°C cooling reconstructed for Greenland (value depends on used calibration [*Alley et al.*, 1997; *Klitgaard-Kristensen et al.*, 1998]) is comparable to the value of 2°–5°C for annual mean temperature depression in our result. Moreover, the simulated strong reduction of precipitation in Greenland (Figure 13) is matching the observation of dry conditions by *Alley et al.* [1997]. Over the North Atlantic and Europe we obtain a cooling of 0.5°–2°C, which is in agreement with estimates of cooling during the 8.2 kyr event for northwestern Europe [*von Grafenstein et al.*, 1998; *Klitgaard-Kristensen et al.*, 1998] and with evidence from Atlantic Ocean cores [*Duplessy et al.*, 1992; *Bond et al.*, 1997; *Labeyrie et al.*, 1999]. In the Nordic seas and Arctic Ocean, a reduced inflow of North Atlantic waters around 8 ka and associated cooling is reported in several studies [e.g., *Cronin et al.*, 1995; *Lloyd et al.*, 1996; *Bauch and Weinelt*, 1997; *Bauch et al.*, 1999], which is consistent with the strong cooling and perennial sea ice cover noted in our results. The decrease in tropical precipitation simulated by the model (Figure 13) is smaller in magnitude than suggested by the widespread fall in lake levels in Africa and Asia [e.g., *Street-Perrott and Perrott*, 1990; *Gasse and Van Campo*, 1994; *Gasse*, 2000]. The same is true for the Scandinavia and the

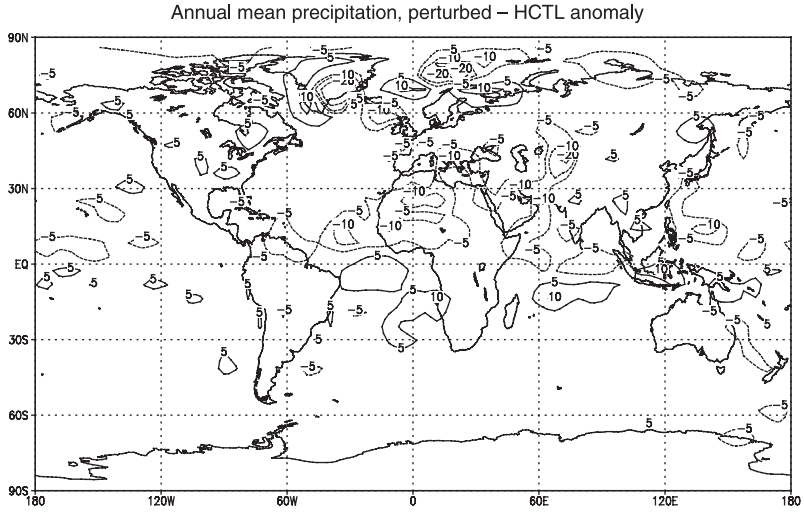

Figure 13. Annual mean precipitation anomaly (20 year (a) perturbation, HCTL). Contours are at −30, −20, −10, −5, 5, and 10 cm yr^{-1}.

Great Lakes region in North America, where dry conditions have been inferred for the 8.2 kyr event [*Rea et al.*, 1994; *Dahl and Nesje*, 1996; *Alley et al.*, 1997]. However, the windy conditions in North America and Greenland as well as the increase in trade wind strength over the tropical Atlantic found in some records [e.g., *Hughen et al.*, 1996] are captured reasonably well by the model (Figure 14). On the basis of the general agreement with proxy data we conclude that the simulated climatic changes associated with the freshwater pulses are realistic.

4.4. Comparison With Other Model Studies

[25] How do our results compare with freshwater perturbation experiments performed by others? Regarding the amount of freshwater released, our experiments are similar to the one described by *Manabe and Stouffer* [1995]. They perturbed the Geophysical Fluid Dynamics Laboratory (GFDL) fully coupled GCM by releasing a freshwater pulse of 1 Sv during a 10 year period (i.e., 3.11×10^{14} m^3 in total) into the North Atlantic Ocean between 50° and 70°N. In the latter study the THC weakened rapidly, as the maximum North Atlantic overturning rate decreased from 17 to 6 Sv in 10 years (in our cases, from 21 to 16 Sv). Subsequently, a rapid fluctuation of several decades occurred, with a strong increase in the strength of the THC and a northward advection of surface waters with high SSS and SST values. After the initial recovery, the THC rapidly weakened again. This fluctuation is also visible in our results (see, e.g., Figures 11a and 11b). *Manabe and Stouffer* [1995] suggested that the initial THC strengthening was associated with the low density of the injected freshwater mass, which prevented the surface waters from sinking at relatively southerly latitude, thus producing a northward advection of warm surface waters. Following the fluctuation, the THC gradually recovered to its preperturbed state

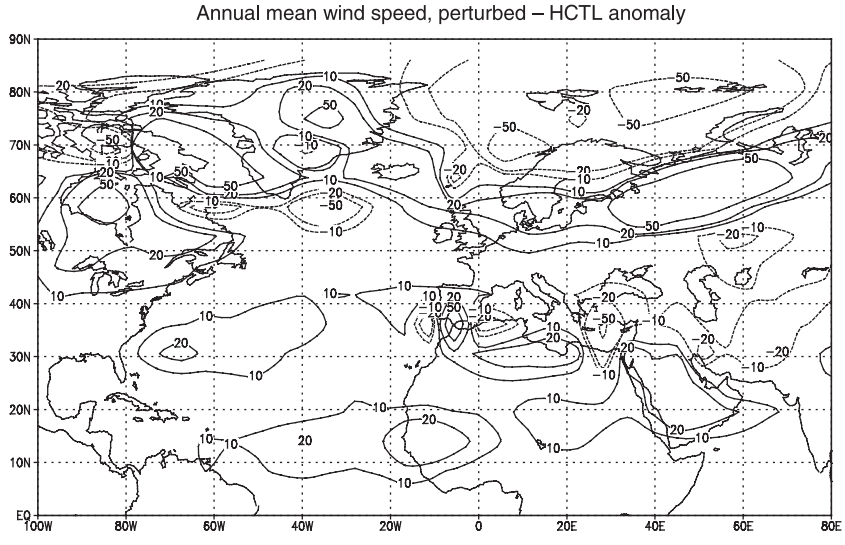

Figure 14. Annual mean wind strength anomaly (20 year (a) perturbation, HCTL) as percentage compared to HCTL. Contours are at −50, −20, −10, 10, 20, and 50%.

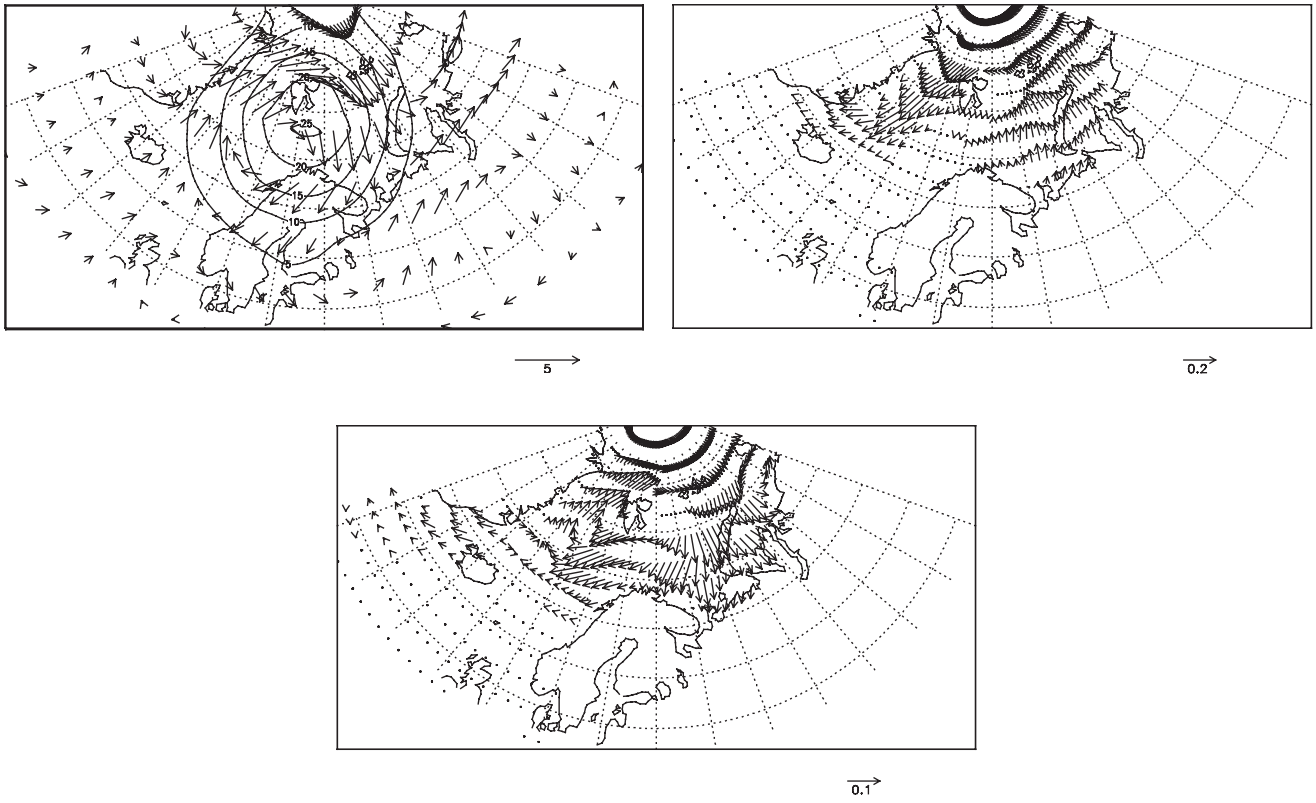

Figure 15. Feedback between atmosphere and sea ice in the Nordic seas. (a) March anomalies (perturbed, HCTL) in atmospheric surface pressure (hPa, contours) and resulting winds (vectors), (b) March sea ice drift in HCTL, and (c) March sea ice drift anomaly (perturbed, HCTL). Note arrow below the plots for scale in m s^{-1}.

after ~200 years, which is more gradual than in our simulations. Although the THC weakening is much stronger than in our cases, the associated surface cooling is comparable. In another experiment, *Manabe and Stouffer* [1997] have perturbed the same model with a more gradual pulse of 0.1 Sv during 500 years (i.e., 1.56×10^{15} m^3 in total, ~3 times our pulse). In the latter experiment the THC is weakened to a maximum North Atlantic overturning rate of 4 Sv at the end of the pulse, after which the model recovers in ~250 years. It is noteworthy that multidecadal fluctuations in SSS, SST, and convection are observed in this experiment, which were absent in their earlier study [*Manabe and Stouffer*, 1995]. The structure of the multidecadal fluctuations resembles the oscillations found in our results, but the duration (~20 years) is longer than in our case (7–11 years in example of Figure 11). As noted by *Tziperman* [2000a, 2000b], this high variability is typical for unstable modes of the THC.

[26] *Weaver* [1999] used an OGCM coupled to an energy-moisture balance model to study the effect of freshwater pulses associated with iceberg influxes. He perturbed a glacial equilibrium state (maximum Atlantic meridional overturning rate of 10 Sv) with two pulses: 0.013 Sv during 105 years (4×10^{13} m^3 in total) and 0.005 Sv during 510 years (8×10^{13} m^3). Surprisingly, the duration of the overturning weakening is similar with these two pulses (~800 years), whereas the maximum overturning rate is reduced to 3.5 and 5.0 Sv for the long and short pulses, respectively. This result led *Weaver* [1999] to conclude that the duration of the THC weakening is determined by internal advective and diffusive processes rather than by the timescale of the perturbation. Our results suggest that Weaver performed too few experiments to draw this conclusion. Our 50, 20, and 10 year freshwater pulses are equivalent to a SSS reduction of 2–4 psu over the North Atlantic north of 40°N. This SSS reduction is comparable to the Atlantic freshening that *Seidov and Maslin* [1999] prescribed in their experiments (with an oceanic circulation model) aimed at studying the effect of Heinrich events during the last glacial. In their case, however, the surface freshening was introduced to a glacial model equilibrium with deep convection in the North Atlantic south of Iceland. Moreover, the freshening was continued for 500 years, making their experiments not really comparable to ours. *Seidov and Maslin* [1999] found that a freshening introduced in the North Atlantic centered at 50°N was much more effective in weakening the THC than a similar freshening that was confined to the Nordic Seas. In other freshwater perturbation studies the design is also very different compared to our experiments, for instance, with freshwater release rates that vary in time or with much larger fluxes than in our case [e.g., *Rahmstorf*, 1995; *Schiller et al.*, 1997; *Mikolajewicz et al.*, 1997; *Fanning and Weaver*, 1997; *Crucifix et al.*, 2001; *Ganopolski and Rahmstorf*, 2001; *Rind et al.*, 2001].

4.5. Implications of Results

[27] Our findings have important implications for other model studies and for the interpretation of proxy records. In contrast to earlier suggestions [e.g., *Manabe and Stouffer*, 1995], the duration of a THC perturbation event may not be a simple function of the amount of meltwater released. In our simulations, releasing two identical (relatively moderate) pulses to the same steady state climate produced events of 1200 and 200 year duration (i.e., 10 year a and d cases). This may imply, for instance, that longer timescale events such as the Younger Dryas (~1200 year duration) were forced by the same kind of pulse as shorter timescale

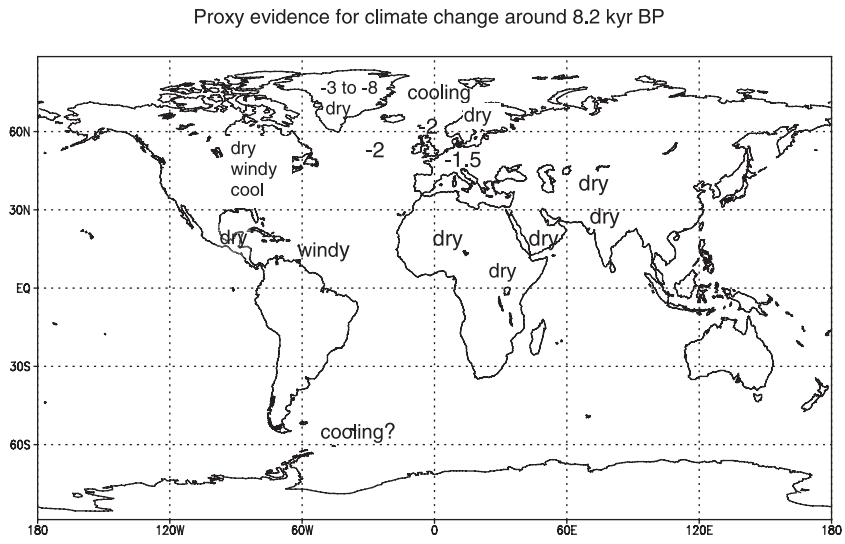

Figure 16. Summary of proxy evidence for climate change at 8.2 ka (partly based on *Alley et al.* [1997] and *Agustdottir* [1998]). The numbers indicate annual mean surface temperature decrease (in °C) compared to early Holocene values. See the text for references that form the basis of this map.

events such as the Older Dryas or the 8.2 kyr event (several 100 years duration). Thus, looking at the paleorecord, it may not always be possible to explain the severity of a climatic event in terms of the magnitude of the forcing. In addition, our results indicate that modelers should be cautious when interpreting results of perturbation experiments, as a particular model outcome is not necessarily unique and other solutions may exist with the same kind of perturbation. Ideally, one should also perform ensemble experiments when studying dynamics of the coupled climate system on longer timescales to ensure that the result is robust.

5. Summary and Conclusions

[28] We have presented the results of experiments in which an early Holocene equilibrium climate state, obtained with a coupled three-dimensional atmosphere–sea ice–ocean model, is perturbed by releasing freshwater pulses into the Labrador Sea, resulting in a weakening of the THC. Three different freshwater pulses have been released at a constant rate: (1) 1.5 Sv in 10 years, (2) 0.75 Sv in 20 years, and (3) 0.3 Sv in 50 years. For each of these pulses we performed five ensemble simulations with different initial conditions, which were sampled from the same early Holocene steady state. The aim was to study in detail the effect of freshwater pulses on the early Holocene climate, thereby referring to the 8.2 kyr event. Our analyses are focused on the effect of high-frequency climate variability on the recovery of the THC. On the basis of the results we conclude the following.

1. Our model produces an early Holocene climate that is consistent with observations and data. Seasonality is strongly increased over middle- and low-latitude continents in response to orbital forcing, yielding seasonal temperatures that differ by several degrees Celsius compared to the modern control climate. In addition, a year-round warming at high latitudes is simulated because of a decrease in sea ice thickness. Moreover, in the tropics, precipitation is enhanced compared to today.

2. In response to the freshwater pulses introduced to the early Holocene climate, two types of overturning recovery have been found in the three sets of ensemble simulations: (1) on a relatively short timescale, $\leq$200 years, and (2) a longer timescale, >200 years. In the experiments with 10 and 20 year pulses both types of recovery were observed, whereas in the 50 year pulse experiments, all recoveries took place within 200 years. The occurrence of the type of recovery appears to follow a statistical probability function, with a longer timescale recovery becoming more likely when the duration of the freshwater pulse becomes shorter. This implies that the type of recovery is unpredictable, at least within the range of parameters studied here. We propose that the unpredictability is linked to high-frequency (annual to decadal) climate variability, as expressed in large fluctuations in sea surface salinity, temperature, and convective activity. These results should be confirmed by studies with other coupled models, as we cannot exclude that our conclusions are model dependent and are influenced by simplifications and parameterizations.

3. A perennial sea ice cover over the Nordic seas stabilizes the perturbed mode through a positive feedback involving the atmospheric circulation. The surface pressure over the Nordic seas increases due to intense surface cooling, causing an increase in sea ice transport from the Barents Sea to the main site of deep convection. This sea ice transport represents an increase in freshwater input, thus lowering the density of the surface waters.

4. The perturbed climate state represents a climate that is in general agreement with the proxy evidence for the 8.2 kyr event in the North Atlantic region and North Africa. This result further supports the hypothesis that a freshwater-induced overturning weakening caused the 8.2 kyr event. Furthermore, it suggests that the simulated climatic changes associated with the freshwater perturbations are realistic.

5. Assuming that our results are sound, they imply that modelers should be cautious in interpreting results on a centennial-to-millennial timescale. Several types of response to the same perturbations may exist. Likewise, the interpretation of paleoclimatic events observed in proxy records may not be as straightforward as believed until now. The strength and duration of a climatic event caused by an overturning weakening may not be simply linearly related to the magnitude of the forcing.

[29] **Acknowledgments.** The authors would like to thank D. Seidov and E. Rohling for thorough reviews of the manuscript. T. Fichefet and H. Goosse are Research Associate and Senior Research Assistant with the National Fund for Scientific Research (Belgium), respectively. This work was done partly within the scope of the Environment and Climate

Programme of the European Commission (contract ENV4-CT97-0643) and the Second Multiannual Scientific Support Plan for a sustainable development policy of the Belgian Federal Office for Scientific, Technical and Cultural Affairs (contract EV/10/9A). The numerical simulations were performed with support of the FNRS Belgium (Fonds de la recherche fondamentale collective-FRFC "project 2.4556.99 'Simulations numériques et traitement des données'"). All of this support is gratefully acknowledged. The authors wish to thank the Data Assimilation Office at the Goddard Space Flight Center, Greenbelt, Maryland, for producing the reanalysis data, and Goddard's Distributed Active Archive Center for distributing the data.

References

Adams, J. M., and H. Faure (Eds.), Review and atlas of palaeovegetation: Preliminary land ecosystem maps of the world since the Last Glacial Maximum, Oak Ridge Natl. Lab., Oak Ridge, Tenn., 1997.

Agustdottir, A. M., Abrupt climate changes and the effects of North Atlantic deepwater formation: Results from the GENESIS global climate model and comparison with data from the Younger Dryas event and the event at 8200 years BP and the present, Ph.D. thesis, Pa. State Univ., University Park, 1998.

Alley, R. B., P. A. Mayewski, T. Sowers, M. Stuiver, K. C. Taylor, and P. U. Clark, Holocene climatic instability—A prominent, widespread event 8200 yr ago, *Geology*, *25*, 483–486, 1997.

Anderson, J. L., and J. J. Ploshay, Impact of initial conditions on seasonal simulations with an atmospheric general circulation model, *Q. J. R. Meteorol. Soc.*, *126*, 2241–2264, 2000.

Barber, D. C., A. Dyke, C. Hillaire-Marcel, A. E. Jennings, J. T. Andrews, M. W. Kerwin, G. Bilodeau, R. McNeely, J. Southon, M. D. Morehead, and J.-M. Gagnon, Forcing of the cold event of 8,200 years ago by catastrophic drainage of Laurentide lakes, *Nature*, *400*, 344–348, 1999.

Bauch, H. A., and M. S. Weinelt, Surface water changes in the Norwegian Sea during last deglacial and Holocene times, *Quat. Sci. Rev.*, *16*, 1115–1124, 1997.

Bauch, H. A., H. Erlenkeuser, K. Fahl, R. F. Spielhagen, M. S. Weinelt, H. Andruleit, and R. Henrich, Evidence for a steeper Eemian than Holocene sea surface temperature gradient between Arctic and sub-Arctic regions, *Palaeogeogr. Palaeoclimatol. Palaeoecol.*, *145*, 95–117, 1999.

Berger, A. L., Long-term variations of daily insolation and Quaternary climatic changes, *J. Atmos. Sci.*, *35*, 2363–2367, 1978.

Blunier, T., J. Chappellaz, J. Schwander, B. Stauffer, and D. Raynaud, Variations in atmospheric methane concentration during the Holocene epoch, *Nature*, *374*, 46–49, 1995.

Bond, G., W. Showers, M. Cheseby, R. Lotti, P. Almasi, P. deMenocal, P. Priore, H. Cullen, I. Hajdas, and G. Bonani, A pervasive millennial-scale cycle in North Atlantic Holocene and glacial climates, *Science*, *278*, 1257–1266, 1997.

Brankovic, C., T. N. Palmer, and L. Ferranti, Predictability of seasonal atmospheric variations, *J. Clim.*, *7*, 217–237, 1994.

Bryan, F., High-latitude salinity effects and interhemispheric thermohaline circulation, *Nature*, *323*, 301–304, 1986.

Campin, J.-M., and H. Goosse, Parameterization of density-driven downsloping flow for a coarse-resolution ocean model in z-coordinate, *Tellus, Ser. A*, *51*, 412–430, 1999.

Chappellaz, J., T. Blunier, S. Kints, A. Dällenbach, J.-M. Barnola, J. Schwander, D. Raynaud, and B. Stauffer, Changes in the atmospheric CH_4 gradient between Greenland and Antarctica during the Holocene, *J. Geophys. Res.*, *102*, 15,987–15,997, 1997.

Charles, C. D., and R. G. Fairbanks, Evidence from Southern Ocean sediments for the effect of North Atlantic deep-water flux on climate, *Nature*, *355*, 416–419, 1992.

Claussen, M., et al., Earth system models of intermediate complexity: Closing the gap in the spectrum of climate system models, *Clim. Dyn.*, *18*, 579–586, 2002.

Cronin, T. M., T. R. Holtz Jr., R. Stein, R. Spielhagen, D. Fütterer, and J. Wollenburg, Late Quaternary paleoceanography of the Eurasian Basin, Arctic Ocean, *Paleoceanography*, *10*, 259–281, 1995.

Crucifix, M., P. Tulkens, and A. Berger, Modelling abrupt climatic changes during the last glaciation, in *The Oceans and Rapid Climate Change: Past, Present and Future*, *Geophys. Monogr. Ser.*, vol. 126, edited by D. Seidov, B. J. Haupt, and M. Maslin, pp. 117–134, AGU, Washington, D. C., 2001.

Crucifix, M., M. F. Loutre, P. Tulkens, T. Fichefet, and A. Berger, Climate evolution during the Holocene: A study with an Earth system model of intermediate complexity, *Clim. Dyn.*, *19*, 43–60, 2002.

Cuffey, K. M., G. D. Clow, R. B. Alley, M. Stuiver, E. D. Waddington, and R. W. Saltus, Large Arctic temperature change at the Wisconsin-Holocene glacial transition, *Science*, *270*, 455–458, 1995.

Dahl, S. O., and A. Nesje, A new approach to calculating Holocene winter precipitation by combining glacier equilibrium-line altitudes and pine-tree limits: A case study from Hardangerjøkulen, central southern Norway, *Holocene*, *6*, 381–398, 1996.

Deleersnijder, E., and J. M. Campin, On the computation of the barotropic mode of a free-surface world ocean model, *Ann. Geophys.*, *13*, 675–688, 1995.

Duplessy, J. C., L. Labeyrie, M. Arnold, M. Paterne, J. Duprat, and T. C. E. van Weering, Changes in surface salinity of the North Atlantic Ocean during the last deglaciation, *Nature*, *358*, 485–488, 1992.

Fanning, A. F., and A. J. Weaver, Temporal-geographical meltwater influences on the North Atlantic conveyor: Implications for the Younger Dryas, *Paleoceanography*, *12*, 307–320, 1997.

Fichefet, T., and M. A. Morales Maqueda, Sensitivity of a global sea ice model to the treatment of ice thermodynamics and dynamics, *J. Geophys. Res.*, *102*, 12,609–12,646, 1997.

Ganopolski, A., and S. Rahmstorf, Rapid changes of glacial climate simulated in a coupled climate model, *Nature*, *409*, 153–158, 2001.

Gasse, F., Hydrological changes in the African tropics since the Last Glacial Maximum, *Quat. Sci. Rev.*, *19*, 189–211, 2000.

Gasse, F., and E. Van Campo, Abrupt post-glacial climatic events in west Asia and North Africa monsoon domains, *Earth Planet. Sci. Lett.*, *126*, 435–456, 1994.

Gloersen, P., W. J. Campbel, D. J. Cavalieri, J. C. Comiso, C. L. Parkinson, and H. J. Zwally, Arctic and Antarctic sea ice, 1978–1987: Satellite passive-microwave observations and analysis, *Rep. NASA SP-511*, NASA, Washington, D. C., 1992.

Goosse, H., and T. Fichefet, Importance of ice-ocean interactions for the global ocean circulation: A model study, *J. Geophys. Res.*, *104*, 23,337–23,355, 1999.

Goosse, H., and H. Renssen, A two-phase response of the Southern Ocean to an increase in greenhouse gas concentrations, *Geophys. Res. Lett.*, *28*, 3469–3472, 2001.

Goosse, H., E. Deleersnijder, T. Fichefet, and M. England, Sensitivity of a global ocean-sea ice model to the parameterization of vertical mixing, *J. Geophys. Res.*, *104*, 13,681–13,695, 1999.

Goosse, H., F. M. Selten, R. J. Haarsma, and J. D. Opsteegh, Decadal variability in high northern latitudes as simulated by an intermediate-complexity climate model, *Ann. Glaciol.*, *33*, 525–532, 2001.

Goosse, H., F. M. Selten, R. J. Haarsma, and J. D. Opsteegh, A mechanism of decadal variability of the sea-ice volume in the Northern Hemisphere, *Clim. Dyn.*, *19*, 61–83, 2002.

Hillaire-Marcel, C., A. deVernal, G. Bilodeau, and A. J. Weaver, Absence of deep-water formation in the Labrador Sea during the last interglacial period, *Nature*, *410*, 1073–1077, 2001.

Hughen, K. A., J. T. Overpeck, L. C. Peterson, and S. Trumbore, Rapid climate changes in the tropical Atlantic region during the last deglaciation, *Nature*, *380*, 51–54, 1996.

Klitgaard-Kristensen, D., H. P. Sejrup, H. Haflidason, S. Johnsen, and M. Spurk, A regional 8200 cal. yr BP cooling event in northwest Europe, induced by final stages of the Laurentide ice-sheet deglaciation?, *J. Quat. Sci.*, *13*, 165–169, 1998.

Knutti, R., and T. F. Stocker, Limited predictability of the future thermohaline circulation close to an instability threshold, *J. Clim.*, *15*, 179–186, 2002.

Koç, N., and E. Jansen, Response of the high-latitude Northern Hemisphere to orbital climate forcing: Evidence from the Nordic Seas, *Geology*, *22*, 523–526, 1994.

Koç, N., E. Jansen, and H. Haflidason, Paleoceanographic reconstructions of surface ocean conditions in the Greenland, Iceland and Norwegian seas through the last 14 ka based on diatoms, *Quat. Sci. Rev.*, *12*, 115–140, 1993.

Koç, N., E. Jansen, M. Hald, and L. Labeyrie, Late glacial-Holocene sea surface temperatures and gradients between the North Atlantic and the Norwegian Sea: Implications for the Nordic heat pump, in *Late Quarternary Palaeoceanography of the North Atlantic Margins*, edited by J. T. Andrews et al., *Geol. Soc. Spec. Publ.*, *111*, 177–185, 1996.

Kutzbach, J. E., and R. G. Gallimore, Sensitivity of a coupled atmosphere/mixed ocean model to changes in orbital forcing at 9000 years B.P., *J. Geophys. Res.*, *93*, 803–821, 1988.

Labeyrie, L., H. Leclaire, C. Waelbroeck, E. Cortijo, J.-C. Duplessy, L. Vidal, M. Elliot, B. Le Coat, and G. Auffret, Temporal variability of

the surface and deep waters of the north west Atlantic Ocean at orbital and millennial scales, in *Mechanisms of Global Climate Change at Millennial Time Scales*, *Geophys. Monogr. Ser.*, vol. 112, edited by P. U. Clark, R. S. Webb, and L. D. Keigwin, pp. 77–98, AGU, Washington, D. C., 1999.

Legates, D. R., and C. J. Willmott, Mean seasonal and spatial variability in gauge-corrected, global precipitation, *Int. J. Climatol.*, *10*, 111–127, 1990.

Lenderink, G., and R. J. Haarsma, Variability and multiple equilibria of the thermohaline circulation associated with deep-water formation, *J. Phys. Oceanogr.*, *24*, 1480–1493, 1994.

Lloyd, J., D. Kroon, C. Laban, and G. Boulton, Deglaciation history and palaeoceanography of the western Spitsbergen margin since the Last Glacial Maximum, in *Late Quarternary Palaeoceanography of the North Atlantic Margins*, edited by J. T. Andrews et al., *Geol. Soc. Spec. Publ.*, *111*, 289–0301, 1996.

MacDonald, G. M., et al., Holocene treeline history and climate change across northern Eurasia, *Quat. Res.*, *53*, 302–311, 2000.

Manabe, S., and R. J. Stouffer, Simulation of abrupt climate change induced by freshwater input to the North Atlantic Ocean, *Nature*, *378*, 165–167, 1995.

Manabe, S., and R. J. Stouffer, Coupled ocean-atmosphere model response to freshwater input: Comparison to Younger Dryas event, *Paleoceanography*, *12*, 321–336, 1997.

Manabe, S., and R. J. Stouffer, Are two modes of the thermohaline circulation stable?, *Tellus, Ser. A*, *51*, 400–411, 1999.

Marotzke, J., and J. Willebrand, Multiple equilibria of the global thermohaline circulation, *J. Phys. Oceanogr.*, *21*, 1372–1385, 1991.

Masson, V., et al., Holocene climate variability sin Antarctica based on 11 ice-core isotopic records, *Quat. Res.*, *54*, 348–358, 2000.

Mellor, G. L., and T. Yamada, Development of a turbulence closure model for geophysical fluid problems, *Rev. Geophys.*, *20*, 851–875, 1982.

Mikolajewicz, U., T. J. Crowley, A. Schiller, and R. Voss, Modelling teleconnections between the North Atlantic and North Pacific during the Younger Dryas, *Nature*, *387*, 384–387, 1997.

Mitchell, J. F. B., N. S. Grahame, and K. J. Needham, Climate simulations for 9000 years before present: Seasonal variations and effects of the Laurentide Ice Sheet, *J. Geophys. Res.*, *93*, 8283–8303, 1988.

Opsteegh, J. D., R. J. Haarsma, F. M. Selten, and A. Kattenberg, ECBILT: A dynamic alternative to mixed boundary conditions in ocean models, *Tellus*, *50*, *Ser. A*, 348–367, 1998.

Peltier, W. R., Ice age paleotopography, *Science*, *265*, 195–201, 1994.

Petoukhov, V., A. Ganopolski, V. Brovkin, M. Claussen, A. Eliseev, C. Kubatzki, and S. Rahmstorf, CLIMBER-2: A climate system model of intermediate complexity, part 1, Model description and performance for present climate, *Clim. Dyn.*, *16*, 1–17, 2000.

Rahmstorf, S., Bifurcations of the Atlantic thermohaline circulation in response to changes in the hydrological cycle, *Nature*, *378*, 145–149, 1995.

Rahmstorf, S., On the freshwater forcing and transport of the Atlantic thermohaline circulation, *Clim. Dyn.*, *12*, 799–811, 1996.

Raynaud, D., J.-M. Barnola, J. Chappellaz, T. Blunier, A. Indermühle, and B. Stauffer, The ice record of greenhouse gases: A view in the context of future changes, *Quat. Sci. Rev.*, *19*, 9–17, 2000.

Rea, D. K., T. C. Moore, T. W. Anderson, C. F. M. Lewis, D. M. Dobson, D. L. Dettman, A. J. Smith, and L. A. Mayer, Great Lakes paleohydrology; complex interplay of glacial meltwater, lake levels, and sill depths, *Geology*, *22*, 1059–1062, 1994.

Renssen, H., H. Goosse, T. Fichefet, and J. M. Campin, The 8.2 kyr BP event simulated by a global atmosphere-sea-ice-ocean model, *Geophys. Res. Lett.*, *28*, 1567–1570, 2001.

Rind, D., P. DeMenocal, G. L. Russell, S. Sheth, D. Collins, G. A. Schmidt, and J. Teller, Effects of glacial meltwater in the GISS coupled atmosphere ocean model, 1, North Atlantic Deep Water response, *J. Geophys. Res.*, *106*, 27,335–27,353, 2001.

Schiller, A., U. Mikolajewicz, and R. Voss, The stability of the North Atlantic thermohaline circulation in a coupled ocean-atmosphere general circulation model, *Clim. Dyn.*, *13*, 325–347, 1997.

Schmitz, W. J., On the interbasin-scale thermohaline circulation, *Rev. Geophys.*, *33*, 151–173, 1995.

Schubert, S. D., J. Pjaendtner, and R. Rood, An assimilated data set for Earth science applications, *Bull. Am. Meteorol. Soc.*, *74*, 2331–2342, 1993.

Schulz, H., Sea-surface temperatures 10,000 years B.P.—Consequences of the early Holocene insolation maximum, *Rep. 73*, 156 pp., Geol. Paläontol. Inst., Univ. Kiel, Kiel, Germany, 1995.

Seidov, D., and M. Maslin, North Atlantic deep water circulation collapse during Heinrich events, *Geology*, *27*, 23–26, 1999.

Seidov, D., E. Barron, and B. J. Haupt, Meltwater and the global conveyor: Northern versus southern connections, *Global Planet. Change*, *30*, 257–270, 2001.

Stocker, T. F., The seasaw effect, *Science*, *282*, 61–61, 1998.

Stocker, T. F., Past and future reorganizations in the climate system, *Quat. Sci. Rev.*, *19*, 301–319, 2000.

Stocker, T. F., and D. G. Wright, Rapid transitions of the ocean's deep circulation induced by changes in surface water fluxes, *Nature*, *351*, 729–732, 1991.

Street-Perrott, F. A., and R. A. Perrott, Abrupt climate fluctuations in the tropics: The influence of Atlantic Ocean circulation, *Nature*, *343*, 607–612, 1990.

Tartinville, B., J. M. Campin, T. Fichefet, and H. Goosse, Realistic representation of the surface freshwater flux in an ice-ocean general circulation model, *Ocean Modell.*, *3*, 95–108, 2001.

Terray, L., S. Valcke, and A. Piacentini, OASIS 2.2, Ocean Atmosphere Sea-ice Soil users's guide and reference manual, *Tech. Rep. TR/CGMC/98-05*, Cent. Eur. de Rech. et de Formation en Calcul Sci. Avancé (CERFACS), Toulouse, France, 1998.

Tziperman, E., Inherently unstable climate behaviour due to weak thermohaline ocean circulation, *Nature*, *386*, 592–595, 1997.

Tziperman, E., Proximity of the present-day thermohaline circulation to an instability threshold, *J. Phys. Oceanogr.*, *30*, 90–104, 2000a.

Tziperman, E., Uncertainties in thermohaline circulation response to greenhouse warming, *Geophys. Res. Lett.*, *27*, 3077–3080, 2000b.

Veum, T., E. Jansen, M. Arnold, I. Beyer, and J.-C. Duplessy, Water mass exchange between the North Atlantic and the Norwegian Sea during the past 28,000 years, *Nature*, *356*, 783–785, 1992.

von Grafenstein, U., H. Erlenkeuser, J. Müller, J. Jouzel, and S. Johnsen, The cold event 8200 years ago documented in oxygen isotope records of precipitation in Europe and Greenland, *Clim. Dyn.*, *14*, 73–81, 1998.

Wang, Z. M., and L. A. Mysak, A simple coupled atmosphere-ocean-sea ice-land surface model for climate and paleoclimate studies, *J. Clim.*, *16*, 1150–1172, 2000.

Weaver, A. J., Millennial timescale variability in ocean/climate models, in *Mechanisms of Global Climate Change at Millennial Time Scales*, *Geophys. Monogr. Ser.*, vol. 112, edited by P. U. Clark, R. S. Webb, and L. D. Keigwin, pp. 285–300, AGU, Washington, D. C., 1999.

Weaver, A. J., P. B. Duffy, M. Eby, and E. C. Wiebe, Evaluation of ocean and climate models using present-day observations and forcing, *Atmos. Ocean*, *38*, 271–301, 2000.

T. Fichefet and H. Goosse, Institut d'Astronomie et de Géophysique Georges Lemaître, Université catholique de Louvain, 2 Chemin du Cyclotron, B-1348 Louvain-la-Neuve, Belgium.

H. Renssen, Faculty of Earth and Life Sciences, Vrije Universiteit Amsterdam, De Boelelaan 1085, NL-1081 HV Amsterdam, Netherlands. (renh@geo.vu.nl)